Journal of Imaging Science and Technology® 55(3): 030509-1–030509-10, 2011.

Spectral Imaging of the Human Retina and Computationally Determined Optimal Illuminants for Diabetic Retinopathy Lesion Detection

Pauli Fält, Jouni Hiltunen and Markku Hauta-Kasari
InFotonics Center Joensuu, University of Eastern Finland, Joensuu Campus, Yliopistokatu 2, P.O. Box 111, FI-80101 Joensuu, Finland
E-mail: pauli.falt@uef.fi

Iiris Sorri and Valentina Kalesnykiene
Department of Ophthalmology, Kuopio University Hospital and University of Eastern Finland, Kuopio Campus, Yliopistonranta 1, P.O. Box 1627, FI-70211 Kuopio, Finland

Juhani Pietilä
Mehiläinen Eye Surgery Clinic, Itäinenkatu 3, FI-33210 Tampere, Finland

Hannu Uusitalo
Department of Ophthalmology, Tampere University Hospital and University of Tampere, Kalevantie 4, FI-33014 University of Tampere, Finland

Abstract. *An ophthalmic fundus camera was modified for spectral imaging of the human retina. Spectral channels were separated using 30 narrow bandpass interference filters in the visual range from 400 to 700 nm. A monochrome digital charge-coupled device camera was used as a detector. Using this system, spectral fundus images were recorded from 72 voluntary human subjects: 55 diabetic patients and 17 healthy control subjects. Furthermore, using the gathered spectral data, optimal illuminations' spectral power distributions for the detection of different lesions of diabetic retinopathy and retinal landmarks (e.g., macula) were calculated. Optimized illuminations were found to enhance the visibility and contrast of retinal features. Computational example images are presented. © 2011 Society for Imaging Science and Technology.*
[DOI: 10.2352/J.ImagingSci.Technol.2011.55.3.030509]

INTRODUCTION

A spectral image is a three-dimensional matrix with two spatial dimensions and one spectral dimension. In other words, every spatial pixel of a spectral image holds a spectrum (e.g., reflectance spectrum) along the third dimension. Different methods for recording spectral images of the ocular fundus have been developed. The reason for measuring spectral images, which can contain tens or hundreds of spectral channels, instead of traditional three-channel red-green-blue (RGB) or one-channel grayscale images, is the superiorly vast and detailed information content. For example, a reflectance spectral image provides accurate spectral color information of each pixel in the image.

Received Aug. 10, 2010; accepted for publication Jan. 8, 2011; published online Apr. 4, 2011.
1062-3701/2011/55(3)/030509/10/$20.00.

Many researchers have done reflectance measurements of the ocular fundus by measuring either a single spectrum from a point[1,2] or several spectra from a line.[3,4] Delori et al. used a fundus camera system (FCS) together with an external xenon-arc lamp/filter wheel combination to take fundus photographs with 11 filters on a black and white film.[5] Faulkner and Kemp used a FCS and five interference filters to record a video of the fundus with a television camera.[6]

In previous studies, Delori and Burns used a fundus spectrophotometer to measure fundus reflectance from a relatively small 3° diameter retinal field in order to estimate the density of the crystalline lens.[7,8] Styles et al. used a liquid crystal tunable filter (LCTF) together with a FCS and steady-state broadband light source to record fundus spectral images.[9] Their method produced spectral images with an adequately large field-of-view, showing the ocular fundus and high spectral resolution of 400–700 nm at 10 nm intervals. Unfortunately, due to the characteristics of the LCTF, this method suffered from long exposure times, up to 5 s per spectral channel, and from fuzzy images that resulted from continuous involuntary eye movement of the human subject during the long nonstop imaging process.

Khoobehi et al. used a FCS combined with a line-measuring spectral camera with a spectral range from 410 to 950 nm to measure the oxygen saturation of the optic nerve head from the eyes of two anesthetized monkeys.[10] This system recorded the spectral image one line at a time and is not directly applicable to the measurement of the ocular fundus of an awake human subject.

Johnson et al. developed a diffractive optical element (DOE) based snapshot spectral imaging FCS, which took a

single image containing multiple spectral channel images from the range of 450–700 nm.[11] However, the construction of a spectral image from the DOE-based image required complicated post-processing and calibration.

Bone et al. used a FCS and a relatively complex system of multibandpass filters, prisms, and charge-coupled devices (CCDs) to take four-band spectral images of the retina.[12] Beach et al. used a FCS together with a simultaneous dual-wavelength imaging system.[13] Ramella-Roman et al. studied the oxygen saturation in the human retina, also using a FCS and a custom built multiaperture camera that was able to capture six spectral channel images on a CCD array.[14] These three systems were specialized to measure only certain wavelength channels and did not give detailed spectral color information of the retina.

In diabetes, high blood glucose level (hyperglycemia) causes metabolic, functional, and structural changes in retinal vascular system, neuroglia, and neurons usually called diabetic retinopathy.[15] The first structural ophthalmoscopically or photographically detectable signs of diabetic retinopathy are microaneurysms and small hemorrhages. These two are generally called small red dots, because it is usually difficult to separate them from each other. Damaged blood vessels also release plasma into the retina, which can cause edema (swelling). As a sign of plasma leakage, yellowish hard lipid exudates form in the retina. The occlusion of small arterioles results in nonperfusion areas (retinal microinfarcts) and formation of soft exudates and intraretinal microvascular abnormalities. Oxygen deprivation leads to an expression of angiogenetic growth factors like vascular endothelial growth factor and finally to real proliferative retinopathy with neovascularization in the retina and vitreous body.[16] Unfortunately, as these novel vessels are thin and fragile, they often break and bleed in the retina and into the vitreous phase.

Practically all long-time diabetics suffer from some degree of retinopathy. Progressive retinopathy will lead to loss of vision if left untreated.[17] The treatment of diabetic retinopathy requires highly educated eye care professionals, high-cost equipment, regular screening, and follow-up. All of these, combined with other diabetes-related complications, place an enormous and ever-growing burden on countries' health care systems and economies. For the optimal treatment, early detection of diabetic retinopathy is very important.

We have developed a FCS-based imaging system for measuring spectral images of the ocular fundus. The proposed spectral imaging method gave high spatial resolution images of the fundus with relatively simple off-the-shelf equipment (filters, external light source, CCD camera). Our system is similar to that of Delori et al.,[5] but our instrumentation is more modern and the number of filters is higher.

Our imaging system uses a set of 30 narrow bandpass interference filters to separate spectral channels from the wavelength range of 400–700 nm. For the safety and comfort of the patient, the filters are placed between the light source and the retina. The imaging system was used to acquire spectral fundus images from 72 voluntary human subjects: 55 diabetics and 17 nondiabetic control subjects. The spectral fundus image database based on these measurements was presented in our previous work.[18]

Furthermore, in this study, spectral color information is used to optimize the spectral power distribution (SPD) of an illumination which maximizes the contrast between a retinal feature (e.g., microaneurysm) and the surrounding healthy tissue. The efficient particle swarm optimization (PSO) algorithm is used to obtain the optimal illumination SPDs.[19,20] The optimal illuminations are calculated for the following cases: (1) microaneurysms, (2) hard exudates, (3) microinfarcts, (4) fibrosis, (5) laser photocoagulation scars, and (6) blot bleedings. Furthermore, the optimization is tested in these cases: (7) maximum contrast between macular and nonmacular areas and (8) maximum contrast between arteries and veins. Statistically insignificant spectral regions (outliers) are removed from the resulting SPDs, and computational example images are presented for every case to demonstrate the effect these illuminations would have in retinal imaging.

The results are promising: contrast and visibility were improved in all studied cases versus the green channel of a RGB image. In the scope of this study, only theoretical computational examinations were considered. The main benefit of our approach is that the contrast and visibility of a desired retinal feature could be improved simply by using an illumination with an optimized SPD during the actual retinal imaging. That is, the contrast could be enhanced even without image processing. The results could be used, e.g., to improve the functionality of ophthalmic devices for the detection of retinal features.

EQUIPMENT

Fundus camera systems are used by ophthalmologists and other health care providers in eye clinics and health centers all over the world. The functionality of the system is usually improved with other integrated devices, such as video cameras and monitors. Even though a multidevice system, FCS is usually simply referred to as a "fundus camera."

In this study, a Canon CR5-45NM fundus camera (Canon, Inc.) was modified for spectral imaging (Figure 1). In the developed system, a Schott Fostec DCR III fiber optic illuminator (Schott North America, Inc.) equipped with a 150 W halogen lamp (Osram Corp.) with a daylight-simulation filter served as a light source, providing broadband illumination in the visual range of the electromagnetic spectrum, i.e., wavelengths from 380 to 780 nm. Light was guided into the FCS via a fiber optic cable. A total of 30 narrow bandpass interference filters (Edmund Optics, Inc.) were used one by one to filter the incoming light. These 30 filters had an average full width at half maximum of 10 ± 2 nm, and they spanned the wavelength range of 400–700 nm at approximately 10 nm intervals (see Figure 2). Filters were placed in four acrylic glass filter holders, each holding up to eight filters, with the last one having two empty slots. The use of narrow bandpass filters allowed the

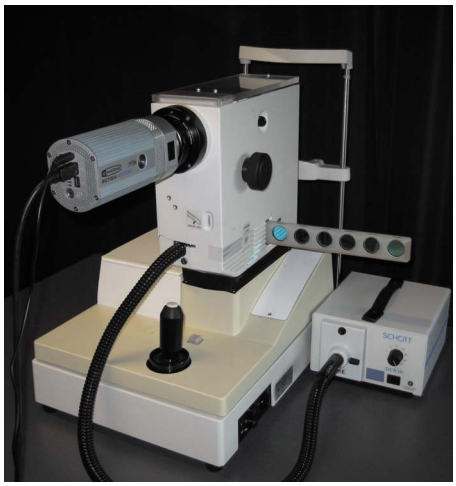

Figure 1. The spectral fundus camera modified from a commercial fundus camera (see the text for details).

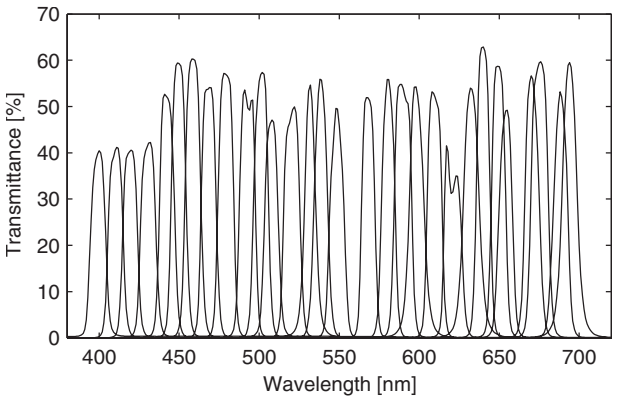

Figure 2. The spectral transmittances of the 30 narrow bandpass interference filters.

measurement of spectral images—and the derivation of the SPDs of the optimal illuminants—with a relatively high spectral resolution.

Several modifications were made to the camera system: First, the microscope part of the device was "stripped down" so that only the fundamental optics remained. The monitor, video camera, and controlling electronics were removed. Second, the original in-built incandescent halogen observation light and xenon flash light sources were removed, and an input opening for a fiber optic cable and a through-the-body opening for filter holders were built to the frame of the FCS. Finally, inside the frame, acrylic glass rails for the filter holders were installed next to the light input. The incoming fiber optic cable was attached to these rails so that the output of the cable was relatively close to an interference filter when a filter holder was placed on the rails. These rails also included a mechanical spring stopper that ensured that the filters were in a correct position in front of the cable output. Filter changing was done manually by sliding a filter holder on the rails until the mechanical stopper locked the holder in a correct place.

A QImaging Retiga-4000RV grayscale digital CCD camera (QImaging Corp.) was used as a detector. The CCD detector array size was 2048×2048 pixels. The camera was mounted to the fundus camera with a standard C-mount adapter. The camera was connected to a standard PC via a Firewire port and was operated with QCAPTURE PRO 6.0 software provided by the manufacturer. From the viewpoint of fundus imaging, this software had many useful functions, such as a live preview window for real time monitoring, calculation of camera exposure time from a user-selected area in the live preview window, possibility to amplify the digital signal (gain), and ability to program the camera to automatically take a desired number of images as quickly as possible (the burst mode). Additionally, as images were taken, they were automatically named and saved to the PC's hard drive, which significantly reduced the duration of an imaging session.

SPECTRAL FUNDUS IMAGING

During the fundus imaging, the light transported into the FCS via the fiber optic cable was immediately filtered by one of the 30 narrow bandpass interference filters. This filtered light was then guided into the patient's eye through FCS's optical system of mirrors and lenses. Patient's pupil was dilated by using a topical application of tropicamide eye drops (Oftan Tropicamid, Santen Oy, Finland) to ensure that the maximum amount of light reached the retina. Light entering the eye transmitted through the ocular media (cornea, aqueous humor, crystalline lens, and vitreous body), reflected from the fundus, and returned through the ocular media back into the FCS, where the reflected light was finally projected on the CCD detector array.

It is important to notice that the illuminating light was filtered before being guided into the eye. This way only approximately 1% of the total radiant power of the broadband light source that reached the eye, which minimized the possibility of photochemical damage to the retina and eliminated the possibility of infrared-based thermal injury (due to the narrow band transmission of the interference filters). Illumination of the fundus with filtered light also made the whole measurement session more patient-friendly. Blinking was encouraged between takings of the images to avoid drying of the cornea.

The fundus imaging procedure was as follows: The external Schott halogen light source was allowed to stabilize for at least 30 min before the beginning of the measurement session. The live preview window of the imaging software was used to determine the correct spatial position of the FCS in relation to the eye. In order to minimize head movements, patient's head was supported against the forehead and chin rests. A fixation target (a small light or a round paper target attached to a wall) was then used to position the eye in a direction where all the key parts of the fundus (papilla, macula, and main vessel branches) were visible. A fixation target was also needed during the actual imaging to minimize involuntary eye movements. Finally, the image was focused by using the in-built focusing controls of the FCS. The eye was illuminated through a green-light-transmitting filter during all these steps.

During the imaging, a filter was placed in the correct position next to the fiber optic output. The patient gazed at the fixation target, and the camera operator subjectively chose the optimal moment to take the image, i.e., the moment when the retina was in focus and in a desired position. The exposure time for the monochrome camera was calculated from a selected area in the preview image: usually a rectangular area enclosing the papilla (with papilla being the most reflective part of the fundus). Sometimes, especially when illuminating the eye with red light, other "plain" parts of the fundus could become highly reflective, so the exposure time was calculated from these areas instead. In practice, the exposure times were varied from 1.25 to 0.04 s, with an average exposure time of 0.2 s.

The gain value for the camera was set to 6, while gamma and offset remained at their default values of 1 and 0, respectively. This gain value was found to be practical since it reduced the camera exposure time without amplifying the noise too much. Exposure times differed from person to person due to different ocular transmittances, but they were usually longest for the violet- (approximately 1 s) and shortest for the red-light-transmitting filters ($<$0.1 s). Digital images were 8-bit grayscale, with an image size of 1024×1024 pixels (using 2×2 binning). Due to the constant involuntary movements of the eye, the camera was programmed to take five consecutive images (per filter) of the retina using the burst mode. The five recorded images were immediately checked by the camera operator; and, if none of them was considered acceptable, a new set of five images was taken using the same filter.

After successfully taking a set of images, the next filter was placed on the optical path, the light was once again guided through the dilated pupil into the eye, and the fundus camera was focused on the retina as much as possible using the focusing dial on the FCS and the live image in the software's preview window. The refocusing, combined with the calculation of the exposure time, usually took at least 30 s, or even a couple of minutes, if the test subject felt it necessary to have a brief pause before the refocusing operation.

The number of retaken five-image sets differed from person to person. The need to retake a set was far more common when the retina was illuminated with violet or blue light than when using red light, because the light source's emission and filter's transmittances of violet light were quite poor, which resulted in long exposure times (up to 1.25 s). Also, with elderly people, the natural age-related yellowing of the crystalline lens reduces the amount of violet/blue light both when the light goes into the eye and when the reflected light comes back out through the lens. Of course, if no information could be gathered from the fundus with the violet-light-passing filters, the image capture began from the first filter in the filter sequence from violet to red that enabled the FCS user to detect landmarks from the retina. If no difficulties were encountered during an imaging session, an experienced user of the FCS could go through the whole set of 30 filters in 20 min. As a reference, 30 spectral channel images were taken from a nonfluorescent Spectralon diffuse white reflectance standard (Labsphere, Inc.), which reflects $>$99% of all light in the visual range.

From each set of five images, one image was chosen. These 30 chosen spectral channel images were registered and stacked into a three-dimensional $1024\times1024\times30$ spectral image. Exposure times of all the images (layers) in the spectral image were normalized to 1 s. No shading or vignetting corrections were applied to the spectral channel images. Each pixel (x,y) in this spectral image contained a spectrum of the form

$$s_{\text{fundus}}(\lambda) = S(\lambda)T_{\text{filter}}(\lambda)T_{\text{FC}}(\lambda)T_{\text{OM}}^2(\lambda)R_{\text{retina}}(\lambda)H_{\text{camera}}(\lambda) + O_{\text{fundus}}(\lambda), \quad (1)$$

where $S(\lambda)$ is the spectral power distribution of the light going to the filter, λ is the wavelength of the electromagnetic radiation, $T_{\text{filter}}(\lambda)$ is the combined spectral transmittance of all the interference filters, $T_{\text{FC}}(\lambda)$ is the total spectral transmittance of the fundus camera optics, $T_{\text{OM}}(\lambda)$ is the spectral transmittance of the ocular media of the eye (second power, because light passes through these media twice), $R_{\text{retina}}(\lambda)$ is the spectral reflectance of the retina, and $H_{\text{camera}}(\lambda)$ is the total spectral sensitivity of the camera. Finally, $O_{\text{fundus}}(\lambda)$ is the offset term that includes the effect of the noise: mostly dark current and stray light.

Analogously, the 30 images taken from the white reflectance standard were normalized and stacked into a spectral image. Unfortunately, the standard's surface was flat, whereas the FCS has been designed to distribute light evenly on a curved surface (eye bottom). Accordingly, white reference images could not be used directly to make the necessary corrections to the spectral fundus images. Instead, a mean spectrum $s_{\text{white}}(\lambda)$ was calculated from a 100×100 pixel area in the white reference spectral image. This spectrum was of the form

$$s_{\text{white}}(\lambda) = S(\lambda)T_{\text{filter}}(\lambda)T_{\text{FC}}(\lambda)R_{\text{white}}(\lambda)H_{\text{camera}}(\lambda) + O_{\text{white}}(\lambda), \quad (2)$$

where $R_{\text{white}}(\lambda)$ is the spectral reflectance of the white standard and $O_{\text{white}}(\lambda)$ is the offset. Let us assume $R_{\text{white}}(\lambda)=1$, $\forall\lambda\in[400,700]$ nm and $O_{\text{fundus}}(\lambda)=O_{\text{white}}(\lambda)=0$, $\forall\lambda\in[400,700]$ nm. The former assumption is justified by the spectral characteristics of the Spectralon coating and the latter by the fact that, in an 8 bit dark image, the average effect of noise was $<$0.4%. Now, from Eqs. (1) and (2) one gets the final spectral image, which holds for every pixel in the image; the spectrum has the form

$$R_{\text{final}}(\lambda) = T_{\text{OM}}^2(\lambda)R_{\text{retina}}(\lambda) = \frac{s_{\text{fundus}}(\lambda)}{s_{\text{white}}(\lambda)}. \quad (3)$$

The transmittance of the ocular media $T_{\text{OM}}(\lambda)$ is unique for each individual; and, to the authors' knowledge, no measurement device exists that could measure it *in vivo*. Thus, the gathered spectral fundus images contain "pseudoreflectance" spectra $T_{\text{OM}}^2(\lambda)R_{\text{retina}}(\lambda)$ according to Eq. (3). From the

viewpoint of ophthalmology, this is not a problem since the effect of the ocular media is always present in practice.

IMAGE REGISTRATION

During the fundus imaging, the test subject's eyes made constant involuntary movements. This caused the resulting spectral channel images to be spatially misaligned with each other. The transformation of partially overlapping images, taken from the same target, into the same coordinate system is called image registration. The automatic image registration algorithm used in this study was the generalized dual-bootstrap iterative closest point (GDB-ICP) algorithm by Stewart and co-workers.[21,22] Image registration was done with publicly available software released by the same group. One of the spectral channel images was selected as a base image that provided the coordinate system into which all the other images were transformed. Occasionally the GDB-ICP software failed with very dark images or images without clear landmarks. These images had to be registered manually by using MATLAB's Control Point Selection Tool (The Mathworks, Inc.).

HUMAN SUBJECTS

A total of 72 voluntary human subjects participated in the fundus imaging trials. These included 55 diabetics (30 females and 25 males) and 17 controls (4 females and 13 males). Ages of the diabetic subjects ranged from 21 to 81 yr with an average age of 56.2 yr. Only one eye was imaged from each subject. The study was conducted in the Department of Ophthalmology in the Kuopio University Hospital (Kuopio, Finland) and was approved by the local research ethics committee of the University Hospital District of Northern Savo. The clinical trials followed the principles of the Declaration of Helsinki, and all the subjects gave their written consent before entering the study.

OPTIMAL ILLUMINANTS FOR DIABETIC RETINOPATHY LESION DETECTION

Optimization Procedure

Since many different kinds of retinal lesions exist, the question arises of what would be the optimal illumination for the detection of a certain lesion type? It is intuitive that only one illuminant is insufficient to optimize the detection of all possible lesions. To solve this problem, the measured spectral data were used together with the PSO algorithm to gain the SPDs of the optimal illuminations for each type of lesion separately.[19,20]

The PSO algorithm is an intuitive optimization routine, in which a "swarm" of particles is randomly initiated in the solution space S. The particles search the solution space S for the optimal point $\hat{\mathbf{g}} \in S$, which minimizes/maximizes the fitness (cost/goal) function $f(\mathbf{x})$. During every step of the algorithm, each individual particle is aware of the current best solution it has found (local best solution, *localBest*) and of the current best solution of the entire swarm (global best solution, *globalBest*). Each particle has velocity v and position x, which are both updated each step t. In this study, the velocity v_i and position x_i of particle i, with $i=1,\ldots,N$, where N is the total number of particles in the swarm, were updated according to the following equations:

$$v_i(t+1) \leftarrow C_0 v_i(t) + C_1 r_1(t)(localBest_i(t) - x_i(t)) + C_2 r_2(t) \times (globalBest(t) - x_i(t)),$$

$$x_i(t+1) \leftarrow x_i(t) + v_i(t+1), \tag{4}$$

where the constant C_0 is called inertia, constants C_1 and C_2 determine how much weight the particle gives to the current *localBest* and *globalBest* solutions, and $r_1(t)$ and $r_2(t)$ are random values from a uniform distribution $U[0,1]$. Particles are updated until convergence, i.e., until the optimal solution $\hat{\mathbf{g}}$ (the final *globalBest*) is found. As is usual with blind-search optimization algorithms, there is a possibility that $f(\hat{\mathbf{g}})$ is only a local minimum/maximum value and $\hat{\mathbf{g}}$ is not the global optimal solution in S. Logically, a large number of particles increase the probability of finding the optimal solution, but are computationally more expensive.

The optimization problem was formulated as follows: Let $\mathbf{s} \in \Re^n$ be the discrete n-dimensional SPD of the illuminant, $\mathbf{F} \in \Re^{n\times n}$ be a matrix that has the spectral transmittances of the narrow bandpass interference filters used in this study on its columns, $\mathbf{r}_1, \mathbf{r}_2 \in \Re^n$ be the spectral reflectances of two separate points on the object, and $\mathbf{h} \in \Re^n$ be the spectral sensitivity of the monochrome detector. In this study, the photopic luminosity function [see Figure 3(e)] was used as $\mathbf{h}$, because it models the human retina's sensitivity to light and many monochrome cameras' spectral sensitivities are similar. This choice increases the generality and usability of the derived SPDs.

Now the intensity value $I_j \in [0,1]$, where $j=1,2$, captured by the detector can be formulated as

$$I_j = k\mathbf{s}^{\mathrm{T}}\mathbf{H}\mathbf{r}_j, \tag{5}$$

where T denotes transpose, matrix $\mathbf{H}=\mathrm{diag}(\mathbf{h})$, and normalization constant $k=1/(\mathbf{s}^T\mathbf{h})$. Additionally, let us define the illuminant's SPD as a convex combination of the light transmitted by the narrow bandpass interference filters:

$$\mathbf{s} = \mathbf{F}\mathbf{a}, \tag{6}$$

where $\mathbf{a} \in \Re^n$ is the weight vector, so that $a_i \geq 0$, $\forall i \in \{1,\ldots,n\}$, and $\Sigma_{i=1}^n a_i = 1$. The filters $\mathbf{F}$ were used in the calculations because that enables the realization of the optimized illuminations in practice. However, in the scope of this study, only computational examples on how the illuminations affect the visibility of the retinal lesions were considered.

Substituting $\mathbf{s}$ in Eq. (5) with Eq. (6), we find that the only unknown parameter for calculating I_j is the convex combination weight vector $\mathbf{a}$. The optimal weight vector $\mathbf{a}$ was solved using PSO as follows: In Eq. (6), a 30-dimensional spectral distribution is expressed as a convex combination of the spectral bands. The PSO algorithm was implemented to seek the optimal weights of this convex

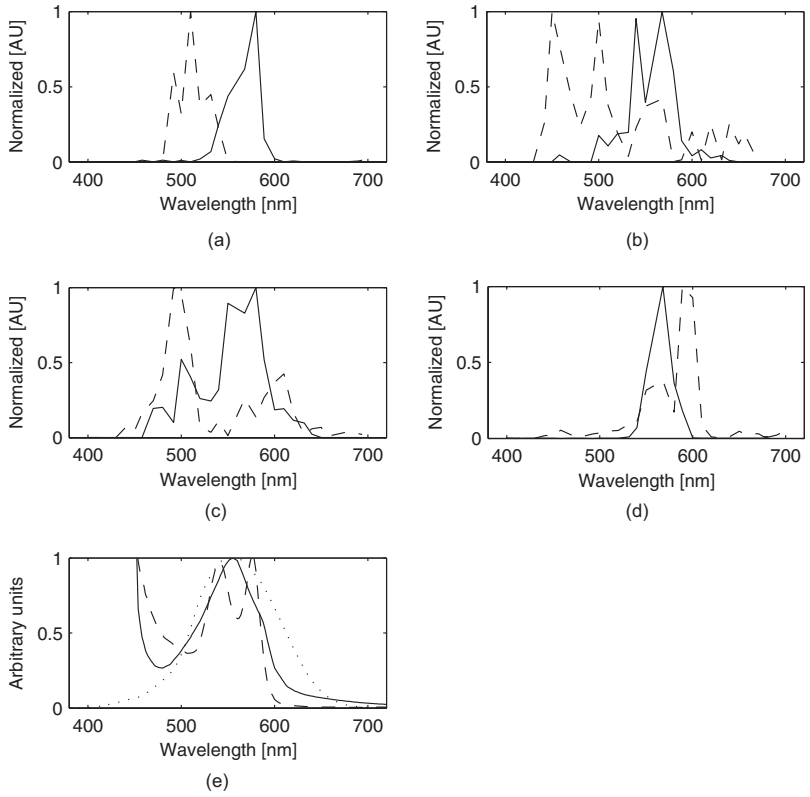

Figure 3. The spectral power distributions of the optimal illuminants for the detection of (a) microaneurysms (solid line), microinfarcts (dashed line), (b) hard exudates (solid line), fibrosis (dashed line), (c) laser photocoagulation scars (solid line), macula (dashed line), (d) blot bleedings (solid line), and arteries vs veins (dashed line). In (e), the photopic luminosity function (dotted line) and the absorption spectra of hemoglobin Hb (solid line) and oxyhemoglobin HbO_2 (dashed line) are shown in arbitrary units.

combination within a 30-dimensional convex hull (solution space). Particles are randomly initialized within the solution space. During every iteration loop, for each particle, a contrast value c (between the intensity values I_1 and I_2) is calculated using the well-known Michelson's formula

$$c = \frac{\max\{I_1, I_2\} - \min\{I_1, I_2\}}{\max\{I_1, I_2\} + \min\{I_1, I_2\}}. \tag{7}$$

As the iteration proceeds, the best solution (highest contrast) particle i has been able to find is saved as $localBest_i$. The *localBest* that produces the highest contrast of all is saved as *globalBest*. The velocity and location of particle i are then updated by using the $localBest_i$ and *globalBest* solutions. After the iteration terminates, the final *globalBest* is the optimal weight vector $\mathbf{a}$ of Eq. (6).

Intensity values I_1 and I_2 were calculated with Eq. (5) using the mean spectra $\mathbf{r}_1$ and $\mathbf{r}_2$ from two separate 3×3 spatial areas in the spectral fundus image, respectively. The area was chosen to be small because many of the lesions in the images were small in size (e.g., some microaneurysms and hard exudates). In Eq. (5), the intensity values were normalized to be within the scale [0,1], so the contrast value c will also be within the same limits. Diabetic lesion/healthy tissue pairs were selected manually from five different sites in every applicable spectral fundus image. The optimal SPD that maximized the contrast value c was calculated for every pair separately by using the PSO algorithm with 100 particles and constants $C_0=0.95$, $C_1=2$, and $C_2=2$ [see Eq. (4)].

Optimal Illuminations

The SPDs of the illuminations were optimized for the following cases: (1) microaneurysms, (2) hard exudates, (3) microinfarcts, (4) fibrosis, (5) laser photocoagulation scars, and (6) blot bleedings. Furthermore, the optimization was tested in these cases: (7) the maximum contrast between macular and nonmacular areas and (8) the maximum contrast between arteries and veins.

Case (1): As stated above, a 3×3 area was chosen manually from a microaneurysm, and analogously from the surrounding healthy tissue (not from the optic nerve head or from the vasculature). The PSO algorithm converged to a solution for the illumination that maximized the contrast between the microaneurysm and the healthy surrounding. This procedure was repeated for five different sites in every applicable spectral fundus image. In order to gain a SPD that would be statistically more reliable, and suitable for many different retinas, all the gained solutions for individual microaneurysms were combined. Microaneurysms were chosen from 53 spectral fundus images (two of 55 diabetic images did not contain any clear microaneurysms), from five different sites in each image, a total of 265 microaneurysm/

healthy tissue pairs. The resulting optimized SPD of the illuminant is displayed in Fig. 3(a).

Case (2): For hard exudates—and for all the other cases—the procedure was identical to case (1). Spectra were extracted from 19 spectral fundus images, from five different sites (a total of 95 hard exudate/healthy tissue pairs). If the number of hard exudates in an image was not sufficient, but the appearing exudates were relatively large in size, points were selected from different areas in the same exudates. The resulting optimized SPD of the illuminant is displayed in Fig. 3(b).

Case (3): Only three spectral fundus images contained clear microinfarcts. The spectra were collected from five different sites in each spectral image (a total of 15 microinfarct/healthy tissue pairs), and the resulting optimized SPD of the illuminant is displayed in Fig. 3(a).

Case (4): The fibrosis spectra were collected from six spectral images at five different points (a total of 30 fibrosis/healthy tissue pairs). The resulting optimized SPD of the illuminant is displayed in Fig. 3(b).

Case (5): With the laser photocoagulation scars, the spectra were taken from the scar tissue and from the surrounding healthy tissue. The spectra were extracted from 13 spectral images, at five different sites (a total of 65 scar/healthy tissue pairs). The resulting optimized SPD of the illuminant is displayed in Fig. 3(c).

Case (6): The blot bleeding spectra were extracted from 15 spectral fundus images, at five different sites (a total of 75 blot bleeding/healthy tissue pairs). The resulting optimized SPD of the illuminant is displayed in Fig. 3(d).

Case (7): In the case of the macula, the spectra were extracted from 71 spectral fundus images (in one image out of the 72, the macula was not clearly visible). Five different sites were chosen from each image, i.e., a total of 355 macular region/nonmacular region pairs. The nonmacular areas were chosen from the healthy fundus background, not from the blood vessels, the optic nerve head, or the lesions. The resulting optimized SPD of the illuminant is displayed in Fig. 3(c).

Case (8): In order to maximize the contrast between arteries and veins, five different artery/vein pairs were selected from each of the 72 spectral fundus images (a total of 360 pairs). The 3×3 areas were chosen from the middle of the vessels. The resulting optimized SPD of the illuminant is displayed in Fig. 3(d).

The SPDs in Fig. 3 show clear characteristic shapes for each different case. Unsurprisingly, in the case of microaneurysms and blot bleedings, the dominating spectral regions are practically exclusively in the range of 540–590 nm. This is due to the absorption of light by hemoglobin as can be seen from Fig. 3(e). The results are in agreement with the use of the so-called "red-free" filters that are commonly used in ophthalmology in order to increase the contrast between the blood-related features and the retinal background. The optimal SPD for microaneurysms centers at 580 nm, around the second major absorption spike of oxyhemoglobin HbO_2. Interestingly, the SPD for blot bleedings, however, centers more on the spectral region of 550–570 nm where the difference between HbO_2 and hemoglobin Hb absorption is largest. This might indicate that the hemoglobin in blot bleedings is mostly deoxygenized since the stronger absorption of Hb could lead to a greater contrast with the surrounding healthy tissue.

From RGB images, veins and arteries can sometimes be difficult to separate from each other visually, but by using certain spectral regions of light, the contrast can be improved. In Figure 6(x) the thick vein appears darker than the surrounding arteries. This result was also expected due to the different absorption characteristics of HbO_2 and Hb in the blood. The optimal SPD has the most significant wavelength regions around 550–570 and 590–600 nm, regions in which the differences between the absorption spectra of HbO_2 and Hb are large.

The SPD for microinfarcts was obtained by maximizing the contrast between 15 microinfarct/healthy tissue pairs. The number of samples is relatively small, but as can be seen from Fig. 3(a), the solutions are all in the wavelength range of 480–550 nm (with the most significant spike at 510 nm). In this blue-cyan region, the healthy surroundings of a microinfarct appear visually darker than in other spectral regions, whereas the whitish infarct remains relatively bright.

The SPD for fibrosis in Fig. 3(b) has characteristic spikes in the violet-blue region. There are relatively a lot of scatters in the solutions, but the spikes at 450 and 500 nm are clearly dominant. As with microinfarcts, the contrast of whitish fibrotic growth versus darker healthy background is maximized at these wavelengths. The scattering of the solutions across the visual range is at least partly due to the low number of samples (30 pairs) and due to the varying thickness and transparency of the fibrotic growth.

There are also some scatters in the solutions for hard exudates and laser photocoagulation scars in Figs. 3(b) and 3(c), which is at least partly explained by their often yellowish-white appearance. Hard exudates and laser scars are relatively strongly reflecting throughout the visual range of light. One reason that the SPDs have significant regions within the 530–600 nm range is that the spectral sensitivity of the detector is highest in this range [see Fig. 3(e)].

The SPD for the detection of the macula is shown in Fig. 3(c), and it has a clear characteristic spike around 490 nm. Here, the visual contrast between the macular and nonmacular regions is likely caused by reflection and scattering of blue light from the inner limiting membrane and the nerve fiber layer, and the natural absorption of violet-blue light by macular pigments.[23] The second region of interest, 550–630 nm, was caused by overly dark spectral channel images in the blue-light region: with elderly patients, the natural age-related yellowing of the crystalline lens of the eye prevents violet-blue light from reaching the retina.[24] Thus, since in these cases the blue-light spectral channels consist mostly of noise, the "second best" solutions are found from the 550–630 nm wavelength range.

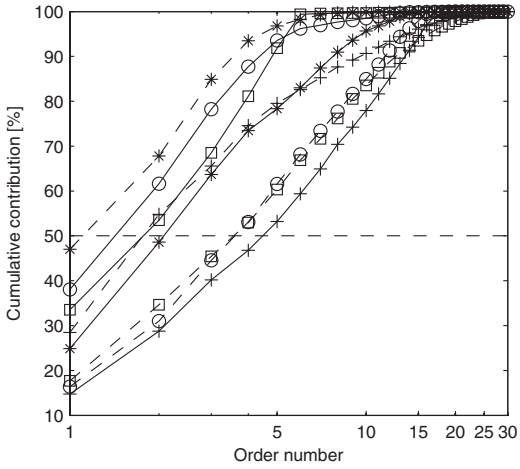

Figure 4. The spectral channels' cumulative contribution to the SPDs of Fig. 3. The most significant spectral channel has the order number 1, and the least significant channel has the order number 30. Cases: microaneurysms (solid line, circles), hard exudates (solid line, asterisks), microinfarcts (solid line, squares), fibrosis (solid line, plus), laser photocoagulation scars (dashed line, circles), blot bleedings (dashed line, asterisks), macula (dashed line, squares), and arteries vs veins (dashed line, plus signs). Also, the 50% limit is presented.

Outlier Removal and Computational Example Images

In all cases of the optimization process, the PSO algorithm converged to a solution which consisted of a singular narrow spectral channel. This is because the illumination SPDs were presented as a combination of light transmitted by the narrow bandpass filters (Fig. 2). In order to remove outliers (i.e., statistically insignificant spectral regions) from the SPDs of Fig. 3, the cumulative contributions of the most significant narrow spectral channels were calculated. The results are shown in Figure 4.

In Fig. 4, the 30 spectral channels were ordered according to their contribution to the SPD, so that the most significant channel is number 1, and the least significant one is number 30 in the graph. In this study, only the first spectral channels which had a cumulative contribution of just over 50% were chosen, and the rest of the channels were omitted. The removed spectral channels were considered as outliers in the solution space S. The filtered spectra are presented in Figure 5.

The 50% limit was found to be adequate, as can be seen from the computational example images in Fig. 6. Images for the optimized illuminations have been calculated from the spectral fundus images according to Eq. (5). For visualization reasons, only small segments of the 1024×1024 fundus images are displayed. Each of images (a)–(x) in Fig. 6 has also been divided by its maximum value. This scaling does not affect the relative level of contrast between the pixels. In all cases, the visual contrast gained with the outlier-free illumination of Fig. 5 was equally good or better than that gained with the original illumination of Fig. 3. Especially, in the case of enhancing the visibility of the macula, the increase in visual contrast is relatively large [see Figs. 6(t) and 6(u)].

Of course, these results are only valid for the chosen detector (in this case, the photopic luminosity function) and in the sense of maximizing local contrast between two manually selected points. Because different eyes have different optical properties, e.g., due to the age-related yellowing of the crystalline lens, the resulting SPDs in Fig. 5 may not be optimal in every possible case, but the SPDs can be considered "statistically optimal."

CONCLUSIONS

Spectral fundus images from the retinas of 72 voluntary human subjects (55 diabetic patients and 17 healthy control subjects) were measured using a modified fundus camera system. The imaging system incorporated 30 narrow band-

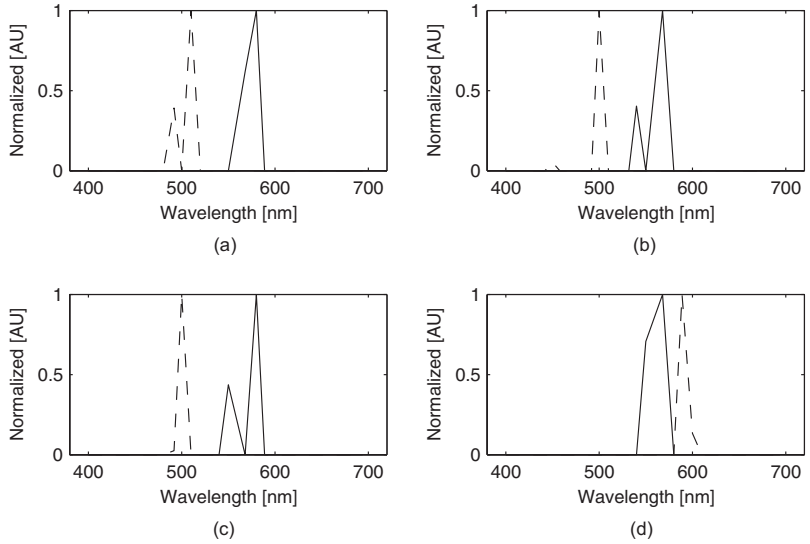

Figure 5. The outlier-free spectral power distributions of the optimal illuminants (see Fig. 3). (a) Microaneurysms (solid line), microinfarcts (dashed line), (b) hard exudates (solid line), fibrosis (dashed line), (c) laser photocoagulation scars (solid line), macula (dashed line), (d) blot bleedings (solid line), and arteries vs veins (dashed line).

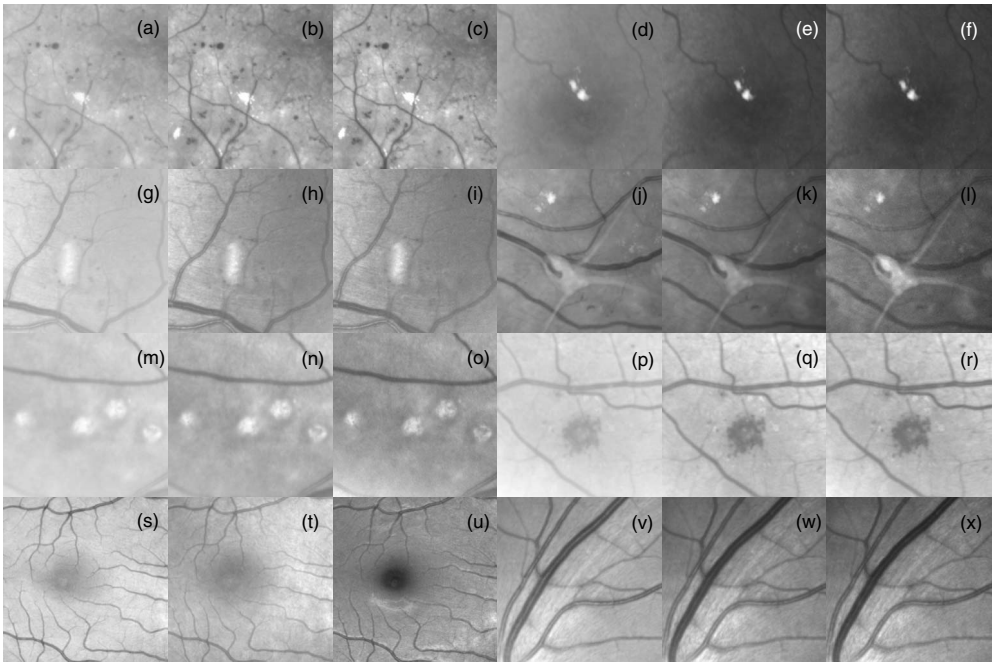

Figure 6. Segments from computational example images demonstrating the effect of the optimized illuminations. Left: green channel of a RGB image; center: effect of the illuminant from Fig. 3; right: effect of the illuminant from Fig. 5. Cases: (a)–(c) microaneurysms, (d)–(f) hard exudates, (g)–(i) microinfarcts, (j)–(l) fibrosis, (m)–(o) laser photocoagulation scars, (p)–(r) blot bleedings, (s)–(u) macula, and (v)–(x) arteries vs veins.

pass interference filters that were used to separate narrow spectral channels from white light in the visual range from 400 to 700 nm. Spectral images were measured from the human ocular fundus since a spectral image contains accurate spectral color information, which, e.g., a standard RGB image does not. A spectral fundus image database based on these measurements was presented in our previous work.[18]

In this article, the illuminations' optimized spectral power distributions for the detection of retinal lesions (e.g., microaneurysms and hard exudates) and other features (e.g., macula) are calculated and computational example images are presented. The optimization is computed by the particle swarm optimization algorithm in the sense of maximizing visual contrast. It is shown that, in retinal imaging, the contrast and visibility of retinal features could be improved by using illuminations with optimized spectral power distributions. Thus, the visibility of the features could be improved even without image processing. The optimized illuminations could be implemented in ophthalmic devices for an improved detection of retinal features.

ACKNOWLEDGMENTS

This work was funded by Tekes, the Finnish Funding Agency for Technology and Innovation under Funding Decision No. 40039/07, Filing No. 2773/31/06 (FinnWell program) and Funding Decision No. 70062/09, Filing No. 2254/31/09. The authors would like to thank Joni Kämäräinen and Lasse Lensu for the original idea. The authors would also like to thank Helvi Käsnänen (Department of Ophthalmology, Kuopio University Hospital) for the recruitment of human subjects and for assistance with the imaging.

REFERENCES

[1] D. Van Norren and L. F. Tiemeijer, "Spectral reflectance of the human eye", Vision Res. **26**, 313–320 (1986).
[2] F. C. Delori and K. P. Pflibsen, "Spectral reflectance of the human ocular fundus", Appl. Opt. **28**, 1061–1077 (1989).
[3] M. Hammer, D. Schweitzer, L. Leistritz, M. Scibor, K.-H. Donnerhacke, and J. Strobel, "Imaging spectroscopy of the human ocular fundus *in vivo*", J. Biomed. Opt. **2**, 418–425 (1997).
[4] M. Hammer and D. Schweitzer, "Quantitative reflection spectroscopy at the human ocular fundus", Phys. Med. Biol. **47**, 179–191 (2002).
[5] F. C. Delori, E. S. Gragoudas, R. Francisco, and R. C. Pruett, "Monochromatic ophthalmoscopy and fundus photography", Arch. Ophthalmol. (Chicago) **95**, 861–868 (1977).
[6] D. J. Faulkner and C. M. Kemp, "Human rhodopsin measurement using a TV-based imaging fundus reflectometer", Vision Res. **24**, 221–231 (1984).
[7] F. C. Delori and S. A. Burns, "Fundus reflectance and the measurement of crystalline lens density", J. Opt. Soc. Am. A **13**, 215–226 (1996).
[8] F. C. Delori, "Spectrophotometer for noninvasive measurement of intrinsic fluorescence and reflectance of the ocular fundus", Appl. Opt. **33**, 7439–7452 (1994).
[9] I. B. Styles, A. Calcagni, E. Claridge, F. Orihuela-Espina, and J. M. Gibson, "Quantitative analysis of multi-spectral fundus images", Med. Image Anal. **10**, 578–597 (2006).
[10] B. Khoobehi, J. M. Beach, and H. Kawano, "Hyperspectral imaging for measurement of oxygen saturation in the optic nerve head", Invest. Ophthalmol. Visual Sci. **45**, 1464–1472 (2004).
[11] W. R. Johnson, D. W. Wilson, W. Fink, M. Humayun, and G. Bearman, "Snapshot hyperspectral imaging in ophthalmology", J. Biomed. Opt. **12**, 014036 (2007).
[12] R. A. Bone, B. Brener, and J. C. Gibert, "Macular pigment, photopigments, and melanin: Distributions in young subjects determined by four-wavelength reflectometry", Vision Res. **47**, 3259–3268 (2007).
[13] J. M. Beach, K. J. Schwenzer, S. Srinivas, D. Kim, and J. S. Tiedeman, "Oximetry of retinal vessels by dual-wavelength imaging, calibration and influence of pigmentation", J. Appl. Physiol. **86**, 748–758 (1999).
[14] J. C. Ramella-Roman, S. A. Mathews, H. Kandimalla, A. Nabili, D. D. Duncan, S. A. D'Anna, S. M. Shah, and Q. D. Nguyen,

"Measurement of oxygen saturation in the retina with a spectroscopic sensitive multi aperture camera", Opt. Express **16**, 6170–6182 (2008).
[15] T. W. Gardner, D. A. Antonetti, A. J. Barber, K. F. LaNoue, and S. W. Levison, "Diabetic retinopathy: More than meets the eye", Surv. Ophthalmol. **47**, S253–S262 (2002).
[16] L. P. Aiello, R. L. Avery, P. G. Arrigg, B. A. Keyt, H. D. Jampel, S. T. Shah, L. R. Pasquale, H. Thieme, M. A. Iwamoto, J. E. Park, H. V. Nguyen, L. M. Aiello, N. Ferrara, and G. L. King, "Vascular endothelial growth factor in ocular fluid of patients with diabetic retinopathy and other retinal disorders", N. Engl. J. Med. **331**, 1480–1487 (1994).
[17] M. Henricsson, A. Nilsson, L. Groop, A. Heijl, and L. Janzon, "Prevalence of diabetic retinopathy in relation to age at onset of the diabetes, treatment, duration and glycemic control", Acta Ophthalmol. Scand. **74**, 523–527 (1996).
[18] P. Fält, J. Hiltunen, M. Hauta-Kasari, I. Sorri, V. Kalesnykiene, and H. Uusitalo, "Extending diabetic retinopathy imaging from color to spectra", *Proceedings of Image Analysis, 16th Scandinavian Conference*, Lecture Notes in Computer Science (LNCS) (Springer, Berlin, 2009) Vol. **5575**, pp. 149–158.
[19] J. Kennedy and R. Eberhart, "Particle swarm optimization", *Proceedings of the IEEE International Conference on Neural Networks* (IEEE, Piscataway, NJ, 1995) pp. 1942–1948.
[20] D. Bratton and J. Kennedy, "Defining a standard for particle swarm optimization", *Proceedings of the IEEE Swarm Intelligence Symposium* (IEEE, Piscataway, NJ, 2007) pp. 120–127.
[21] C. V. Stewart, C.-L. Tsai, and B. Roysam, "The dual-bootstrap iterative closest point algorithm with application to retinal image registration", IEEE Trans. Med. Imaging **22**, 1379–1394 (2003).
[22] G. Yang, C. V. Stewart, M. Sofka, and C.-L. Tsai, "Registration of challenging image pairs: Initialization, estimation, and decision", IEEE Trans. Pattern Anal. Mach. Intell. **29**, 1973–1989 (2007).
[23] J. T. Landrum and R. A. Bone, "Lutein, zeaxanthin, and the macular pigment", Arch. Biochem. Biophys. **385**, 28–40 (2001).
[24] E. R. Gaillard, L. Zheng, J. C. Merriam, and J. Dillon, "Age-related changes in the absorption characteristics of the primate lens", Invest. Ophthalmol. Visual Sci. **41**, 1454–1459 (2000).